Journal of Electron Spectroscopy and Related Phenomena 184 (2011) 296–300

Contents lists available at ScienceDirect

Journal of Electron Spectroscopy and Related Phenomena

journal homepage: www.elsevier.com/locate/elspec

Effect of humidity on individual SnO_2 coated carbon nanotubes studied by *in situ* STXM

Jian Wang[a,*], Jigang Zhou[a,*], Haitao Fang[b], Tsun-Kong Sham[c,*], Chithra Karunakaran[a], Yingshen Lu[a], Glyn Cooper[d], Adam P. Hitchcock[d,*]

[a] Canadian Light Source Inc., University of Saskatchewan, Saskatoon, SK S7N 0X4, Canada
[b] School of Materials Science and Engineering, Harbin Institute of Technology, Harbin, Heilongjiang 150001, China
[c] Department of Chemistry, The University of Western Ontario, London, ON N6A 5B7, Canada
[d] Brockhouse Institute for Materials Research, McMaster University, Hamilton, ON L8S 4M1, Canada

ARTICLE INFO

Article history:
Available online 22 December 2010

Keywords:
in situ STXM
Relative humidity (RH)
NEXAFS
SnO_2/CNT
Stack Fit

ABSTRACT

In situ Scanning Transmission X-ray Microscopy (STXM) with humidity control at the 10ID-1 spectromicroscopy beamline at the Canadian Light Source was used to study the effect of humidity on individual SnO_2 coated carbon nanotubes (SnO_2/CNT). O 1s STXM image stacks of individual SnO_2 coated CNT were measured at controlled relative humidity (RH). At high RH = 0.78, 10–50 nm of condensed water was found adsorbed on individual SnO_2/CNT as determined by spectral curve fitting to O 1s image sequences. Coating variations among individual SnO_2/CNT were found. This is consistent with O 1s NEXAFS spectra extracted from the same individual SnO_2/CNT. For some entangled SnO_2/CNT regions, as much as 200 nm condensed liquid water was detected, indicating strong interaction between SnO_2 and water.

1. Introduction

Since their discovery, carbon nanotubes (CNT) have been used for a wide range of applications because of their unique structure and excellent mechanical, electronic, thermal, and chemical properties. Modification of CNT with functional groups, nanostructures or nanomaterials has further inspired significant improvements of these properties relevant to various technological applications [1,2]. Recently, increasing attention has been paid to coating CNT with metal oxides since CNT have proved to be an excellent substrate for these materials [3–12]. Tin oxide (SnO_2) is an important functional material with many remarkable physical and chemical properties itself, including high receptivity variation in gases, low electrical resistivity, high optical transparency and excellent chemical stability. Coating SnO_2 on carbon nanotubes (CNT) dramatically enhances these properties due to reduced aggregation of the SnO_2 nanoparticles, the mesoporous character of the composite material, and the improved conductivity caused by the interaction between SnO_2 and CNT. SnO_2/CNT composites have been used in many applications to achieve better performance, including gas sensors [13–16], catalysts for biosensors [17], catalyst carriers for fuel cells [18], and anode material in Li-ion batteries [19]. For most of these applications, relative humidity (RH) is an important experimental parameter as SnO_2 is sensitive to the presence of water. High-sensitivity humidity sensors based on a single SnO_2 nanowire have been demonstrated [20]. In that study, the electrical resistance of the SnO_2 nanowire decreased linearly and promptly with increased humidity, which implies a strong interaction between SnO_2 and the adsorbed water molecules. In this work, we use *in situ* Scanning Transmission X-ray Microscopy (STXM) with humidity control at the CLS 10ID-1 spectromicroscopy beamline to study the effect of humidity on SnO_2 coated carbon nanotubes (SnO_2/CNT). The objectives are to spectromicroscopically image and quantify water adsorption to individual SnO_2/CNT, and to demonstrate the application of the humidity controlled device for STXM. Specifically, O 1s STXM image stacks of individual SnO_2/CNT were measured at controlled relative humidity. Quantitative chemical maps of the composite material as well as the adsorbed water were obtained by fitting the stacks with NEXAFS reference spectra of the pure components.

This paper is organized as follows: Section 2 presents sample preparation, experimental set up, and data analysis procedure. Section 3 presents the STXM results and the derived quantitative chemical mapping of the water adsorbed SnO_2/CNT sample. This is followed by discussion (Section 4) and conclusion (Section 5).

* Corresponding authors.
E-mail addresses: jian.wang@lightsource.ca (J. Wang), jigang.zhou@lightsource.ca (J. Zhou), tsham@uwo.ca (T.-K. Sham), aph@mcmaster.ca (A.P. Hitchcock).

0368-2048/$ – see front matter © 2010 Elsevier B.V. All rights reserved.
doi:10.1016/j.elspec.2010.12.014

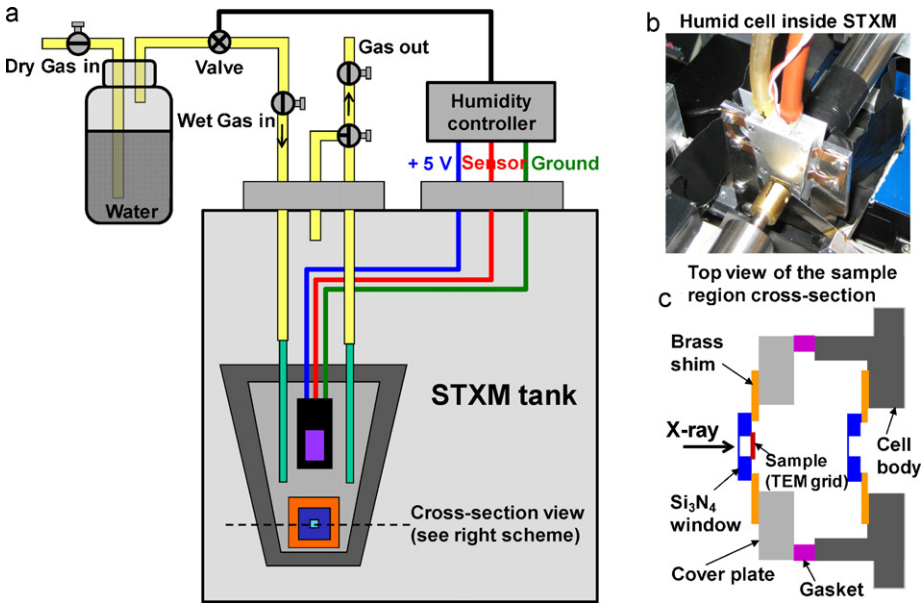

Fig. 1. (a) Schematic of CLS STXM humid cell experimental apparatus; (b) picture of the humid cell inside STXM; and (c) schematic of the top view of the sample region (cross-section of the humid cell).

2. Experimental

2.1. Sample preparation

Multi-walled carbon nanotubes were obtained from Shenzhen Nanotech Port Co. Ltd. with a diameter distribution of 60–100 nm and a claimed purity of 95%. The CNT were treated by refluxing in nitric acid (40%) at 110 °C for 2 h to increase their surface chemical activity via oxidation of the defect sites before coating with SnO_2. Such partially oxidized CNT are referred to as O-CNT. SnO_2 coated carbon nanotubes (SnO_2/CNT) were prepared by a sol-gel reaction using $SnCl_2{\cdot}2H_2O$ as the precursor [3,21]. The as-prepared and dried SnO_2/CNT were deposited onto a holey amorphous carbon TEM grid, which was mounted inside the STXM humidity control device for *in situ* STXM measurements (see more detail below). Pure O-CNT and SnO_2 powder (obtained from Aldrich) were deposited on Si_3N_4 windows (thickness 100 nm, Norcada Inc.) to acquire NEXAFS reference spectra by STXM.

2.2. In situ STXM

In situ STXM was carried out using the scanning transmission X-ray microscope (STXM) at the spectromicroscopy beamline at the Canadian Light Source [22]. The beamline is equipped with an APPLE II type Elliptically Polarizing Undulator (EPU), which provides circularly polarized light (130–1000 eV), and fully plane polarized light (130–2500 eV) with polarization adjustable from −90° to +90°. Left circularly polarized light was used in this study in order to remove any linear dichroism effect originating from different orientations of the CNT [23]. STXM uses a Fresnel zone plate to focus monochromated soft X-rays to a small probe (30 nm in this work). The sample is raster-scanned with synchronized detection of transmitted X-rays to create images. *In situ* humidity control in STXM requires the use of an enclosed cell with humidity monitoring and control [24]. Fig. 1a and b shows the schematic and a picture of the CLS STXM humid cell set up, respectively. Two Si_3N_4 windows (membrane dimensions 0.5 mm × 0.5 mm, thickness 100 nm, Norcada Inc.) are glued to the front and back sides of the humid cell to allow soft X-ray transmission though the cell. They are strong enough to withstand 1 atmospheric pressure. Humidity is monitored *in situ* by a Honeywell HIH-4000 series humidity sensor, which is connected to a custom built humidity controller outside of the STXM tank. The humidity controller adjusts an electrically controlled proportional flow valve to control the flow rate of a wet helium gas stream to achieve an RH equal to the user defined set point. Fully saturated humidity (RH = 1.0) could be achieved only when the cell was outside the STXM as the temperature inside STXM is about 6 °C higher than outside (due to heat generated from various motor stages). Since the wet helium gas is saturated at the lower outside temperature (20.5 °C), the maximum RH that the cell can achieve inside STXM (26.5 °C) is 0.78, i.e. 18 Torr H_2O partial pressure in 1 atm helium carrier gas; and this RH was used for this study. The sample, SnO_2/CNT deposited on a holey amorphous carbon TEM grid, was mounted in the humid cell as shown in Fig. 1c. NEXAFS spectra and chemical maps were obtained from STXM image sequence (stack) scans [25]. For this study O 1s image stacks were recorded from 525 to 560 eV with an energy step of 0.2 eV around the NEXAFS peaks and energy steps between 0.5 and 1.0 eV in the pre-edge and the continuum. The stack dimensions were defined to include CNT sample region of interest, typically a few microns including some blank Io regions. The image pixel size was 25 nm and dwell time was 1 ms per pixel.

2.3. Data analysis

STXM data was analyzed by aXis2000 [26]. The details of principles and procedures of STXM data analysis were described in the supplemental materials of our previous work [27,28]. Briefly, STXM stacks were analyzed by stack alignment, converted to optical density (i.e. absorbance) by normalization to the blank Io regions in the same stack, and fitted with NEXAFS spectra of the pure reference compounds to generate quantitative maps of the chemical components by the aXis2000 stack fit routine, which is based on singular value decomposition (SVD) analysis [29]. The reference spectra were extracted from STXM image stacks of pure materials at uniform regions with suitable thickness. Furthermore, the NEXAFS reference spectra are placed on quantitative intensity scales by scaling the original NEXAFS spectra to match their calculated elemental

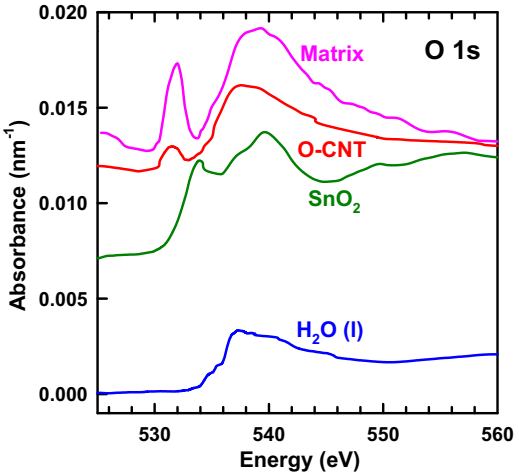

Fig. 2. NEXAFS reference spectra of O-CNT, SnO_2, H_2O(l) and the matrix (holey amorphous carbon) at the O 1s edge. (All spectra are scaled to per nm thickness.)

linear X-ray absorption profiles (with known chemical composition and density) in the pre-edge and the continuum [27]. For components with unknown chemical composition, the linear reference spectra can be obtained approximately by dividing the original spectra with an estimated sample thickness. For the system studied in this work, the reference compounds are considered to comprise O-CNT, SnO_2, H_2O(l) and the holey amorphous carbon. Although H_2O(g) was present in the humid cell, after a careful examination it showed that H_2O(g) was evenly distributed throughout the cell, so after normalization to the Io spectrum (which contains the H_2O(g) spectrum) obtained from blank regions of the image stack, the final optical density stack of the sample does not show H_2O(g) signal in the SnO_2/CNT regions. Moreover, the NEXAFS spectra extracted from the water adsorbed SnO_2/CNT clearly revealed that the adsorbed water is in the condensed phase (details are presented in the following section).

3. Results

Fig. 2 presents O 1s NEXAFS reference spectra of O-CNT, SnO_2, H_2O(l) and the matrix (i.e. holey amorphous carbon) acquired from pure materials. The reference spectra of SnO_2 and liquid water, H_2O(l), were converted to absolute linear absorbance (nm^{-1}) by fitting their original spectra to their elemental linear X-ray absorption profiles with known chemical formula and density. The O 1s spectra of the oxygen functionalized carbon nanotube (O-CNT) and the matrix were scaled to linear absorbance (nm^{-1}) based on an estimate of the average material thickness at the measured regions because the exact chemical composition for these two materials is not known. The features of the O 1s spectrum of O-CNT clearly confirm that oxygen-containing functional groups were generated on the carbon nanotube surface, which are a key to further functionalization of O-CNT by other species [3–12]. For the O 1s spectrum of SnO_2, the first feature at 533.9 eV is assigned to transitions to a state where O 2p orbitals are hybridized with Sn 5s while the second feature at 539.7 eV is assigned to transitions to a state where O 2p orbitals are hybridized with Sn 5p [30]. The small shoulder at 537.5 eV is probably associated with the surface defects related to excess oxygen [31]. The liquid water O 1s spectrum is featured by a major peak at 537.4 eV, assigned to O 1s $\rightarrow \sigma_{O-H}{}^*$ transitions, while the gas phase water O 1s spectrum consists of four discrete peaks at 534.0, 535.9, 537.2, and 538.6 eV [32] of mainly Rydberg character with the 535.9 eV peak most dominant than others. The O 1s spectrum of the holey amorphous carbon matrix shows that there is a significant amount of oxygen present, and the intense peak at 531.9 eV (due to O 1s $\rightarrow \pi^*_{COOH}$ transitions) suggest most oxygen groups are carboxylic groups.

Fig. 3 shows the *in situ* STXM quantitative chemical mapping results of SnO_2/CNT inside the humid cell with RH = 0.78 at 26.5 °C. Fig. 3a presents the map of the O-CNT component. Most of the SnO_2/CNT tubes have intensities corresponding to between 50 and 100 nm indicating that there has been strong oxidation of CNT during the coating process. Fig. 3b and c presents the quantitative thickness distributions of SnO_2 and the adsorbed condensed water H_2O(l), respectively. Fig. 3d is a rainbow color representation of Fig. 3c with 16 levels to provide a better view of the thickness distribution for the adsorbed water. The SnO_2 intensities on/around the CNT show that there is a range of 10–30 nm SnO_2 coated on the individual CNT, demonstrating coating variations among them. Under the specific RH used in this work, 10–50 nm condensed water was adsorbed on individual SnO_2/CNT (Fig. 3c and d), which indicated water adsorption variations among the individual SnO_2/CNT. Furthermore, some entangled SnO_2/CNT regions (upper left side of Fig. 3c and d) show much higher intensities of condensed water (as much as 200 nm), suggesting strong interaction between SnO_2 and water. Fig. 3e shows the shape and areas of the matrix material, which support the SnO_2/CNT deposits. Comparing Fig. 3c–e shows moderate amounts of condensed water are evenly distributed on the matrix areas, implying non-selective adsorption of water on the matrix. An overview of all components is shown in the 4-component colored composite map, Fig. 3f. The individual SnO_2/CNT used for above evaluation of SnO_2 coating thickness and water adsorption amount are highlighted by the white dashed boxes labeled 1–4 in Fig. 3f.

Fig. 4 presents NEXAFS spectra extracted from the image stack at the four individual water adsorbed SnO_2/CNT as indicated in Fig. 3f, compared with the liquid water spectrum. For a better comparison, these spectra were normalized in the O 1s pre-edge and the continuum. A comparison of the spectra clearly shows that tubes 2 and 3 have evident condensed water as indicated by the vertical dashed line located on the liquid water characteristic feature at 537.4 eV in Fig. 4, while tubes 1 and 4 have much less observable spectral features of liquid water. Fig. 4 is consistent with the imaging results in Fig. 3d from which we can see more adsorbed water is associated with tubes 2 and 3 than tubes 1 and 4. However, the SnO_2 coating amount for tubes 2 and 3 is actually less than that of tubes 1 and 4 as shown in Fig. 3b. But the coating looks more uniform for tubes 2 and 3. All these suggest that SnO_2 coating quality is more important to water adsorption than coating amount, and the SnO_2 coating variations and quality are directly reflected by the amount of water adsorption.

4. Discussion

The STXM stack fit procedure to deduce maps requires reference spectra. With quantitative reference spectra, the generated chemical maps are also quantitative. From the results, it is apparent that different amounts of condensed water were adsorbed on different SnO_2/CNT tubes, indicating the expected structure difference between individual SnO_2/CNT, and revealing coating variations among individual CNT. A good SnO_2 coating on CNT exhibits well dispersed and uniform SnO_2 nanoparticles on the CNT surface, which represents a core/shell structure rather than side by side structure as revealed by STXM [21]. The reason for the presence of very high intensities of the condensed liquid water (upper left side of Fig. 3c and d) may be related to strong capillarity action of aggregated pores in the entangled SnO_2/CNT (mesoporous) regions [33]. This work suggests that the individual SnO_2/CNT coating quality and the collective morphology can be probed by water adsorption

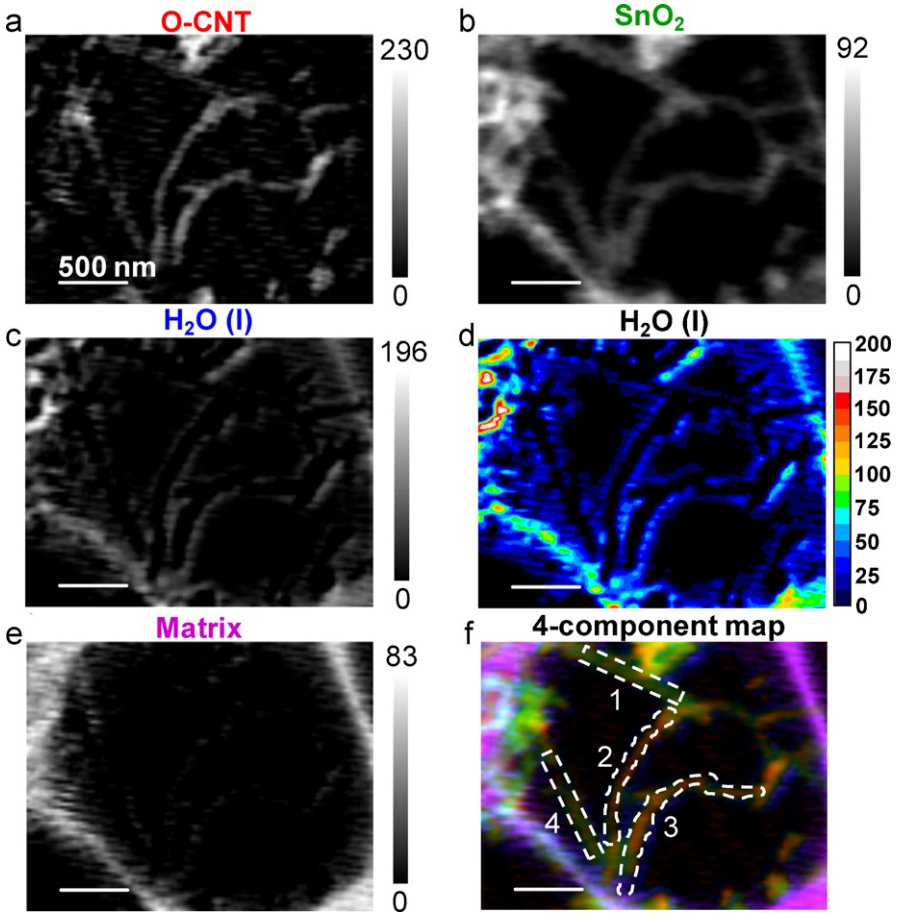

Fig. 3. *In situ* STXM quantitative analysis of SnO_2/CNT inside a humid cell (RH = 0.78, 26.5 °C). Chemical maps of (a) O-CNT (the grey scale represents the thickness of the materials in nm); (b) SnO_2; (c) H_2O(l); (d) 16-level rainbow color image of (c) (the rainbow scale with numbers 0–200 represents liquid water thickness in nm); (e) the holey amorphous carbon matrix; (f) 4-component colored composite map of O-CNT (red), SnO_2 (green), H_2O(l) (blue) and the matrix (purple) with the intensity rescaled in each image channel. Four white dashed boxes labeled 1–4 are individual SnO_2/CNT selected for NEXAFS comparison.

with *in situ* STXM. These findings are important to the development and fabrication of SnO_2/CNT based gas sensors and other similar applications.

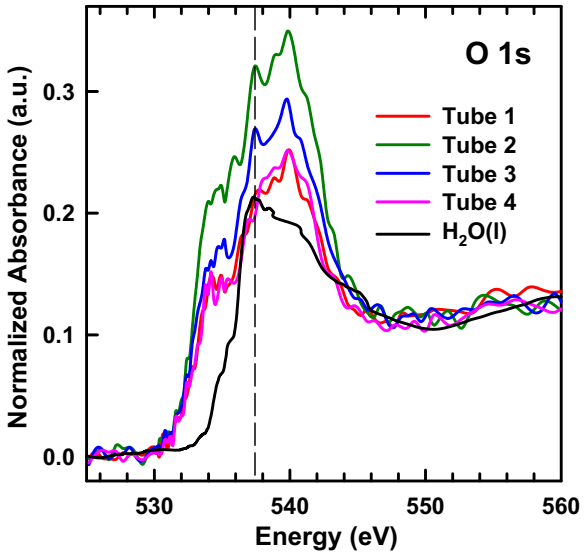

Fig. 4. O 1s NEXAFS spectra of the four individual water adsorbed SnO_2/CNT as indicated by the white dashed boxes in Fig. 3f, compared with the liquid water spectrum. (All spectra are normalized in the O 1s pre-edge and the continuum. The vertical dashed line marks the spectral features of interest.)

5. Conclusion

Under high humidity the behavior of SnO_2 coated CNT was studied by *in situ* STXM. At RH = 0.78, 10–50 nm condensed water was adsorbed on the SnO_2 surface of the individual CNT, demonstrating coating variations among individual SnO_2/CNT. For some entangled SnO_2/CNT regions, as much as 200 nm condensed liquid water is absorbed, implying strong interaction between SnO_2 and water. This study illustrates the unique capacity of STXM in studying single nanostructures under particular environments. This work demonstrates that samples of humid or water sensitive materials can be studied with *in situ* humidity control inside the CLS STXM.

Acknowledgements

This research is supported by Natural Sciences and Engineering Research Council (NSERC) of Canada, Canada Foundation for Innovation (CFI), Canadian Research Chair Program, and National Natural Science Foundation of China (NSFC) (50602011). The Canadian Light Source is supported by CFI, NSERC, Canadian Institutes of Health Research (CIHR), National Research Council (NRC) and the University of Saskatchewan.

References

[1] Y.-P. Sun, K. Fu, Y. Lin, W. Huang, Acc. Chem. Res. 35 (2002) 1096.
[2] H. Chu, L. Wei, R. Cui, J. Wang, Y. Li, Coord. Chem. Rev. 254 (2010) 1117.

[3] H.-T. Fang, X. Sun, L.-H. Qian, D.-W. Wang, F. Li, Y. Chu, F.-P. Wang, H.-M. Cheng, J. Phys. Chem. C 112 (2008) 5790.
[4] Y. Yang, L. Qu, L. Dai, T.-S. Kang, M. Durstock, Adv. Mater. 19 (2007) 1239.
[5] L. Jiang, L. Gao, Mater. Chem. Phys. 91 (2005) 313.
[6] V. Subramanian, H. Zhu, B. Wei, Electrochem. Commun. 8 (2006) 827.
[7] I.-H. Kim, J.-H. Kim, K.-B. Kim, Electrochem. Solid-State Lett. 8 (2005) A369.
[8] Y. Shan, L. Gao, Chem. Lett. 33 (2004) 1560.
[9] L. Fu, Z. Liu, Y. Liu, B. Han, J. Wang, P. Hu, L. Cao, D. Zhu, Adv. Mater. 16 (2004) 350.
[10] I.-H. Kim, J.-H. Kim, B.-W. Cho, K.-B. Kim, J. Electrochem. Soc. 153 (2006) A1451.
[11] Z. Sun, X. Zhang, N. Na, Z. Liu, B. Han, G. An, J. Phys. Chem. B 110 (2006) 13410.
[12] Y. Yu, L.-L. Ma, W.-Y. Huang, J.-L. Li, P.-K. Wong, J.C. Yu, J. Solid State Chem. 178 (2005) 1488.
[13] Y.X. Liang, Y.J. Chen, T.H. Wang, Appl. Phys. Lett. 85 (2004) 666.
[14] Y. Chen, C. Zhu, T. Wang, Nanotechnology 17 (2006) 3012.
[15] Y.-L. Liu, H.-F. Yang, Y. Yang, Z.-M. Liu, G.-L. Shen, R.-Q. Yu, Thin Solid Films 497 (2006) 355.
[16] C. Wongchoosuk, A. Wisitsoraat, A. Tuantranont, T. Kerdcharoen, Sens. Actuators B: Chem. 147 (2010) 392.
[17] F.-F. Zhang, X.-L. Wang, C.-X. Li, X.-H. Li, Q. Wan, Y.-Z. Xian, L.-T. Jin, K. Yamamoto, Anal. Bioanal. Chem. 382 (2005) 1368.
[18] K. Waki, K. Matsubara, K. Ke, Y. Yamazaki, Solid-State Lett. 8 (2005) A489.
[19] J. Xie, V.K. Varadan, Mater. Chem. Phys. 91 (2005) 274.
[20] Q. Kuang, C.S. Lao, Z.L. Wang, Z.X. Xie, L.S. Zheng, J. Am. Chem. Soc. 129 (2007) 6070.
[21] J. Zhou, J. Wang, H. Fang, T.K. Sham, J. Mater. Chem., to be submitted for publication.
[22] K.V. Kaznatcheev, C. Karunakaran, U.D. Lanke, S.G. Urquhart, M. Obst, A.P. Hitchcock, Nucl. Instr. Meth. Phys. Res. A 582 (2007) 96.
[23] E. Najafi, D.H. Cruz, M. Obst, A.P. Hitchcock, B. Douhard, J.J. Pireaux, A. Felten, Small 4 (2008) 2279.
[24] T. Lefevre, M. Pézolet, D. Hernández Cruz, M.M. West, M. Obst, A.P. Hitchcock, C. Karunakaran, K.V. Kaznatcheev, J. Phys. Conf. Ser. 186 (2009) 012089.
[25] C. Jacobsen, S. Wirick, G. Flynn, C. Zimba, J. Microscopy 197 (2000) 173.
[26] http://unicorn.mcmaster.ca/aXis2000.html (available free for non-commercial applications).
[27] J. Zhou, J. Wang, H. Fang, C. Wu, J.N. Cutler, T.K. Sham, Chem. Commun. 46 (2010) 2778.
[28] J. Zhou, J. Wang, H. Liu, M.N. Banis, X. Sun, T.-K. Sham, J. Phys. Chem. Lett. 1 (2010) 1709.
[29] I.N. Koprinarov, A.P. Hitchcock, C.T. McCrory, R.F. Childs, J. Phys. Chem. B 106 (2002) 5358.
[30] C. McGuinness, C.B. Stagarescu, P.J. Ryan, J.E. Downes, D.F. Fu, K.E. Smith, R.G. Egdell, Phys. Rev. B 68 (2003) 165014.
[31] M.S. Moreno, R.F. Egerton, P.A. Midgley, Phys. Rev. B 69 (2004) 233304.
[32] R. McLaren, I. Ishii, A.P. Hitchcock, M.B. Robin, J. Chem. Phys. 87 (1987) 4344.
[33] Q.-H. Yang, P.-X. Hou, S. Bai, M.-Z. Wang, H.-M. Cheng, Chem. Phys. Lett. 345 (2001) 18.